C. R. Physique 19 (2018) 54–63

Contents lists available at ScienceDirect

Comptes Rendus Physique

www.sciencedirect.com

Radio science for Humanity / Radiosciences au service de l'humanité

From quantum physics to digital communication: Single sideband continuous phase modulation ☆

De la physique quantique aux communications numériques : modulation à phase continue et à bande latérale unique

Haïfa Farès [a,b], D. Christian Glattli [b,*], Yves Louët [a], Jacques Palicot [a], Christophe Moy [a], Preden Roulleau [b]

[a] *IETR – UMR CNRS 6164, CentraleSupélec, avenue de la Boulaie, CS 47601, 35576 Cesson-Sévigné cedex, France*
[b] *SPEC UMR 3680 CEA–CNRS, Université Paris-Saclay, CEA Saclay, 91191 Gif-Sur-Yvette, France*

ARTICLE INFO

Article history:
Available online 14 February 2018

Keywords:
CPM
Single side band signal
Low complexity
Orthonormal wave functions
Matched filter

Mots-clés :
Signal à bande latérale unique
Filtrage adapté
Formes d'onde orthonormées
Détection à faible complexité

ABSTRACT

In the present paper, we propose a new frequency-shift keying continuous phase modulation (FSK–CPM) scheme having, by essence, the interesting feature of single-sideband (SSB) spectrum providing a very compact frequency occupation. First, the original principle, inspired from quantum physics (levitons), is presented. Besides, we address the problem of low-complexity coherent detection of this new waveform, based on orthonormal wave functions used to perform matched filtering for efficient demodulation. Consequently, this shows that the proposed modulation can operate using existing digital communication technology, since only well-known operations are performed (e.g., filtering, integration). This SSB property can be exploited to allow large bit rates transmissions at low carrier frequency without caring about image frequency degradation effects typical of ordinary double-sideband signals.

RÉSUMÉ

Dans cet article, nous présentons un schéma de modulation à phase continue basé sur une nouvelle forme d'onde, ayant la propriété de générer directement un signal avec un spectre à bande latérale unique (la bande inférieure ou supérieure à la fréquence porteuse). Tout d'abord, le principe de base de cette nouvelle forme d'onde, issue de la physique quantique, est présenté. Ensuite, une solution au problème de détection cohérente à faible complexité a été dérivée, tout en démontrant que la modulation proposée peut fonctionner en utilisant une technologie de communication numérique existante, étant donné que seules des opérations bien connues sont effectuées (filtrage, intégration…). Cette propriété de bande latérale unique peut être exploitée pour permettre des transmissions à grand débit à faible fréquence porteuse sans se soucier des effets d'interférence avec le spectre image, typiquement connus pour les signaux à double bande latérale.

https://doi.org/10.1016/j.crhy.2018.01.004
1631-0705/

1. Introduction

Communicating with a far-away destination has always been a fundamental concern of mankind. However, not long ago, postal mail remained the only effective means able to perform this function, before the appearance of the telegraph and then the telephone, two major inventions that marked the beginning of the area of telecommunications. From the earliest developments of telephony and radio, the signals are adapted to the transmission channel by means of amplitude or/and phase modulation of a sinusoidal carrier wave. All of these modulation methods are characterized by two-sided signals, that is, a spectrum centered around the carrier frequency having frequency components below and above this carrier frequency. Since the lower band contains the same information as the upper band, one of the most trivial mean for optimizing the spectral occupancy is to keep only one of these two sides by using a bandpass filtering. The Hilbert transform proposed by Hartley in [1] is a simpler mean of suppressing one of the two sidebands, after generating the modulated signal. It consists in constructing, by using a wide-band phase shifter, the sum or difference of the in-phase and quadrature portion of the modulated signal, respectively, to preserve either the upper sideband or the lower sideband. A variant was proposed in [2]. In this paper, we present a new original waveform that directly generates a signal with a single sideband spectrum. By *directly*, we mean without any additional treatment, as described above.

This newly patented modulation is part of the Frequency Shift Keying (FSK) continuous phase modulation (CPM) family, known to be a good candidate to limit the transmitted signal distortion [3,4]. For instance, it generates constant envelope waveforms, which is particularly useful when employing nonlinear amplifiers. The key idea to generate directly a single-sideband modulated signal is the use of a generic frequency pulse with a Lorentzian shape. The Lorentzian shape provides specific properties to a wave, which were found and exploited in fundamental quantum physics for the on-demand injection of a single electron in a quantum conductor as a new excitation called a leviton. This proposed modulation is then suggested as a first application of a classical levitonics to digital transmissions based on CPM. Notwithstanding all these favorable aspects (power efficiency and single sideband transmission), alike current CPM schemes, the proposed modulation scheme, hereafter called Single SideBand Frequency Shift Keying (SSB–FSK), may suffer from implementation complexity. In this paper, we focus on a low-complexity coherent receiver originating from orthonormal wave-functions used to perform matched-filter detection.

This paper is organized as follows. The fundamental modulation principle derived from quantum physics is introduced in Section 2. In Section 3, we briefly describe the system model. Then, a low complexity coherent receiver is detailed in Section 4. Numerical results are reported in Section 5. Finally, in Section 6, we draw some conclusions and define some perspectives.

2. The origin of SSB–FSK modulation: levitons from quantum physics

The ability to control individual electrons in an electronic conductor has been for a long time considered by the community of Quantum Physics as a hot topic. It has been widely investigated in order to pave the way for novel quantum technologies. The topic of on-demand injection of single electrons has been considered using several approaches [5–10]. Here, we consider the technique of voltage pulses applied on a contact to inject a charge in a conductor. The solution, which seems to be trivial, has been implicitly proposed in the theoretical work by Levitov et al [10]. When applying a short voltage pulse $V(t)$ on a contact of a quantum conductor carrying a single electronic mode, an elementary current pulse $I(t) = e^2 V(t)/h_0$ is then generated, where e is the charge of an electron and h_0 is the Planck constant. Adjusting the amplitude and duration of the pulse so as to generate the charge $Q = \int I(t)\,\mathrm{d}t = e$, a single electron is then injected from the contact to the conductor. In general, the voltage pulse perturbs all the electrons of the conductor, resulting in a number of unwanted excitations in the form of electrons (holes) with energy respectively above (below) the Fermi energy of the conductor. Surprisingly, it has been found that a remarkably particular shape of voltage pulses, a Lorentzian and only that shape, excites just a single electron above the Fermi energy. With Lorentzian voltage pulses, a single electron can be injected in the form of an exceptional minimal excitation state called a leviton, where the unwanted excitations are absent. Levitons have been recently produced and observed in [8] using a nanoscale circuit consisting of two electrodes connected by a small conductor. Dubois et al. applied Lorentzian-shaped voltage pulses on one electrode to generate levitons that travel through the conductor to the other electrode [8,9], demonstrating the fundamental prediction of [10]. This major breakthrough has also been exploited to perform the analog of a Hong–Ou–Mandel experiment known from optics, where electrons can be viewed as flying qubits propagating in a ballistic conductor [8]. When a voltage pulse is applied, the phase of electronic quantum waves is modulated as $\varphi(t) = (e/h_0)\int_{-\infty}^{t} V(t')\,\mathrm{d}t'$. The key principle behind the remarkable levitonic quantum state is that, for a Lorentzian pulse, the electron energy spectrum resulting from the phase modulation (their power spectrum density in frequency) becomes *single sideband*. Hence was born the idea of exploiting this original spectral property not only to quantum electronic waves, but also to all types of waves, even classical: electromagnetic, acoustic, etc. [11].

☆ This work was supported by the ERC Proof of Concept 680875 C-Levitonics.

* Corresponding author.
E-mail address: christian.glattli@cea.fr (D. Christian Glattli).

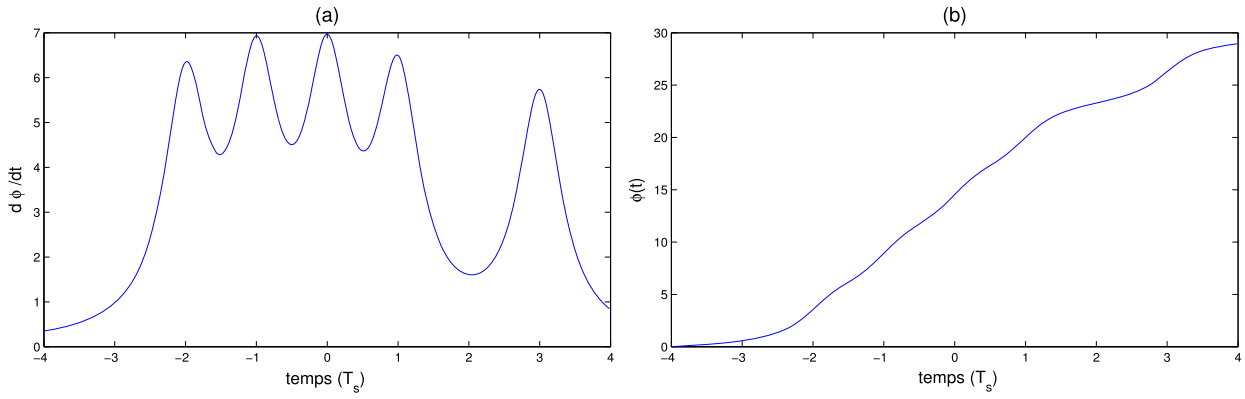

Fig. 1. Generated signals with SSB–FSK modulation of the bit sequence $\{0, 0, 1, 1, 1, 1, 0, 1\}$: (a) Phase derivative (Lorentzian pulses), (b) Evolution of the phase (cumulative phase summing $2\mu a_k \arctan\left(\frac{t-kT_s}{w}\right)$).

3. System model

The signal carrying the binary information is the constant envelope signal given by

$$\begin{aligned} s(t) &= \sqrt{\frac{E_s}{T_s}}\, e^{j(2\pi f_c t+\varphi(t))} \\ &= \sqrt{\frac{E_s}{T_s}}\, e^{j\left(2\pi f_c t+h\sum_{k=-\infty}^{+\infty} a_k \varphi_0(t-kT_s)\right)} \end{aligned} \tag{1}$$

where E_s is the average symbol energy, T_s is the duration of information symbol a_k (taking values in the alphabet $\{0, 1\}$), f_c is the carrier frequency, h is an integer modulation index ensuring a 2π phase increment, $\varphi(t)$ is the phase function and $\varphi_0(t)$ is the elementary Levitonic phase-shift function. To start, we consider frequency pulses truncated to a length L for further ease in demodulation. They are given by

$$\varphi_0(t) = 2\mu(L)\arctan\left(\frac{t}{w}\right) \tag{2}$$

where $\mu(L)$ is a fixed correcting factor that will be defined later.

The derivative of the phase-shift function, $g(t)$, which consists in the frequency pulse, is zero everywhere except in the interval $[-LT_s/2, +LT_s/2]$, where it is a Lorentzian given by

$$\begin{aligned} g(t) &= \frac{d\varphi_0(t)}{dt} = \mu\frac{2w}{t^2+w^2},\ \ t\in[-LT_s/2, LT_s/2] \\ \int_{-t}^{t} g(\tau)\,d\tau &= \varphi_0(LT_s/2) - \varphi_0(-LT_s/2) = 2\pi,\ \ t \geq LT_s/2 \end{aligned} \tag{3}$$

In the sinusoidal signal $s(t)$, we perform a phase coding where the k-th symbol of duration T_s contributes to the total phase $\varphi(t)$ of the carrier by the quantity $2\mu a_k \arctan\left(\frac{t-kT_s}{w}\right)$, where w is the pulse width, a tuning parameter impacting greatly the performance, particularly the spectral efficiency of the transmitted signal $s(t)$. In other words, we associate a Lorentzian pulse with a phase increment equal to $2h\pi$ to symbol 1 and no pulse to symbol 0. The derivative of the total phase is then a sum of Lorentzians $\frac{2\mu w}{(t-kT_s)^2+w^2}$, centered on kT_s and weighted by the symbols a_k and truncated to the length L. Note that if the modulation index h is a positive integer, the spectrum is located only in the upper band with respect to f_c. The modulation index h may also be a negative integer; in this case, we will obtain the mirror spectrum with respect to f_c and no component in this upper band. From this observation, no antipodal coding is possible at the symbol level. Otherwise, the spectrum will return perfectly bilaterally centered around f_c. The components below f_c are representing the contribution of the bits $b_k = 0$ encoded in $a_k = -1$, and the components above f_c are representing the contribution of the bits $b_k = 1$ coded in $a_k = 1$. Fig. 1.(a) shows the phase derivative signal for the bit sequence $\{0, 0, 1, 1, 1, 1, 0, 1\}$; The phase is then integrated to generate the signal of the Fig. 1.(b). This latter shows the continuity of this phase.

Furthermore, given that the Lorentzian pulse decreases very slowly (a 2π phase increment is ensured for $L = \infty$), μ is a correcting factor introduced to keep a 2π phase increment when the frequency pulse $g(t)$ is truncated to a finite $L > 1$

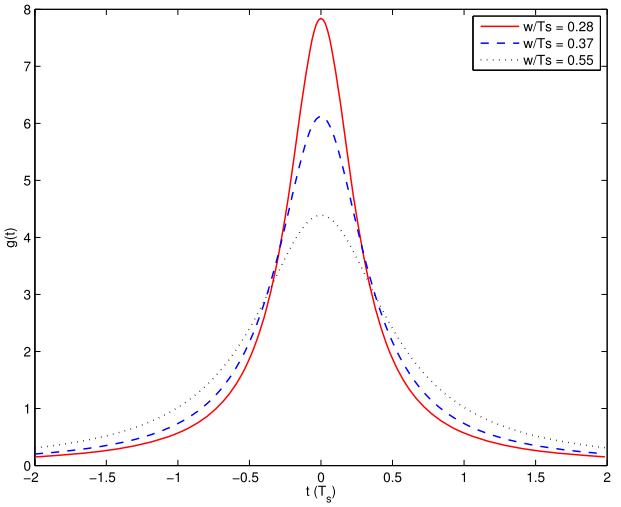

Fig. 2. Length-$4T_s$ frequency pulse: the Lorentzian pulse for different width values, $w/T_s = 0.28, 0.37, 0.55$.

symbol duration. This factor is defined as the ratio between the total phase increment without any truncation and the one obtained after Lorentzian truncation:

$$\mu(L) = \frac{2\pi}{\int_{-LT_s/2}^{LT_s/2} \frac{2w}{t^2+w^2} \mathrm{d}t} = \frac{\pi}{\arctan\left(\frac{LT_s}{2w}\right)} \tag{4}$$

In Fig. 2, we illustrate the Lorentzian pulse for different width values $w/T_s = 0.28, 0.37, 0.55$. As $g(t)$, the frequency pulse is partial response (with long length $L > 1$), so the SSB–FSK modulation exhibits inter-symbol interference (ISI), which is obviously expected and goes up with w. It is therefore imperative to choose a limited width w for Lorentzian pulses to reduce ISI effects on bit error rate (BER) performance.

In order to evaluate the Bit Error Probability (BER) performance, we consider a point-to-point communication system over an additive white Gaussian noise (AWGN) channel. The power-limited input signal **s** (a long sequence of symbols) is summed to the complex noise $\mathbf{z} \sim \mathcal{CN}(0, \sigma_0^2)$ resulting in the output **y**, which is defined, at time t, as

$$y(t) = s(t) + z(t), \tag{5}$$

with σ_0^2 the Gaussian noise variance.

4. Low-complexity coherent detector

In this section, a coherent symbol-by-symbol detection method is presented. This method exploits orthogonality between signals relative to bits 0 and 1. For Matched Filter (MF) based detector, the decision on one symbol is made based on the observation of one received symbol. The memory of CPM signals introduced by the phase continuity can be used to improve BER performance of MF-based detector by making decision on one symbol based on a whole observation window (a sequence of received symbols); this demodulation method is called Average Matched Filter (AMF)-based detection.

4.1. Orthonormal wave-functions

Using $\varphi_0(t)$, a non-truncated Levitonic pulse given in (2) for $\mu = 1$, we define $u_{\tilde{h}}(t)$, $\tilde{h} = 0, 1, 2, ..., N$, from $s_h(t) = \mathrm{e}^{\mathrm{j}h\phi_0(t)}$, a set of orthonormal wave-functions, as

$$\begin{aligned} u_{\tilde{h}}(t) &= \frac{1}{\sqrt{2\pi}} \frac{\mathrm{e}^{\mathrm{j}\tilde{h}\varphi_0(t)}}{t - \mathrm{j}w} \\ &= \frac{1}{\sqrt{2\pi}} \frac{(t + \mathrm{j}w)^{\tilde{h}-1}}{(t - \mathrm{j}w)^{\tilde{h}}} \end{aligned} \tag{6}$$

The set of $\{u_{\tilde{h}}(t)\}$ for all integer h verifies the following orthogonal property:

$$\int_{-\infty}^{+\infty} u_{\tilde{h}}^*(t) u_{\tilde{h}'}(t) \mathrm{d}t = \delta_{\tilde{h},\tilde{h}'} \tag{7}$$

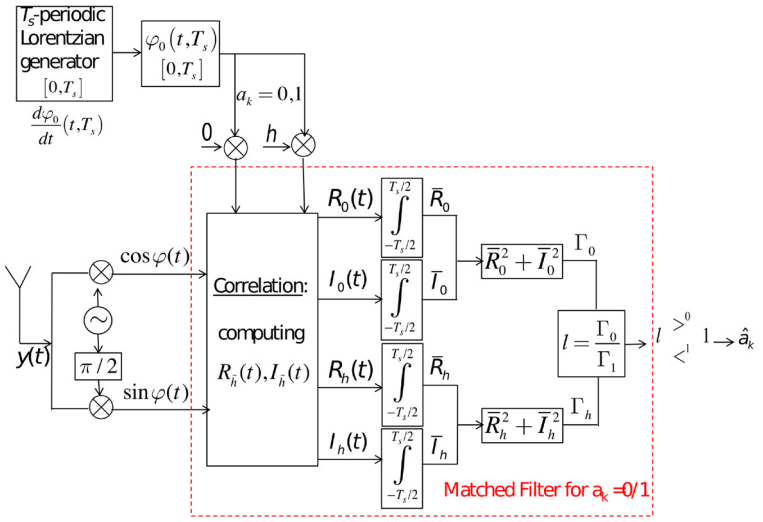

Fig. 3. Block diagram of the MF-based detector.

Based on this interesting observation and remarking that $\frac{\mathrm{d}\phi_0}{\mathrm{d}t} = \frac{1}{(t-\mathrm{j}w)*(t-\mathrm{j}w)}$, we can derive the following equation, which will be central to enable matched-filter detection:

$$\frac{1}{2\pi}\int_{-\infty}^{+\infty} s_{\tilde{h}}^{*}(t)s_{\tilde{h}'}(t)\frac{\mathrm{d}\varphi_0(t)}{\mathrm{d}t}\mathrm{d}t = \delta_{\tilde{h},\tilde{h}'} \tag{8}$$

where $\frac{\mathrm{d}\varphi_0(t)}{\mathrm{d}t}$ is a weighting function and $s_{\tilde{h}}(t)$ is an SSB–FSK modulated signal, which can be rewritten as

$$s_{\tilde{h}}(t) = \mathrm{e}^{\mathrm{j}\tilde{h}\varphi_0(t)} = \left(\frac{t+\mathrm{j}w}{t-\mathrm{j}w}\right)^{h} \tag{9}$$

Furthermore, it is important to notice that even when considering the integration function over a finite period T_s, the orthogonality property, being no longer exact is still quantitatively satisfactorily verified:

$$\frac{1}{2\pi}\int_{-T_s/2}^{+T_s/2} s_{\tilde{h}}^{*}(t)s_{\tilde{h}'}(t)\frac{\mathrm{d}\varphi_0(t)}{\mathrm{d}t}\mathrm{d}t \simeq \delta_{\tilde{h},\tilde{h}'} \tag{10}$$

4.2. Matched-filter-based detector

The block diagram of the proposed MF-based detector is shown in Fig. 3. For binary transmission, matched filtering is inspired from the integration function defined in (10), for $\tilde{h} = ha_k$, where $a_k = 0, 1$. The matched filtering exploits the orthogonality between wave functions of SSB–FSK signals relative to symbols 0 and 1. The detection of the transmitted symbol, using the received signal after the carrier demodulation $\tilde{y}(t)$, is based on the computation of the following correlation functions for $\tilde{h} = 0, h$

$$\Gamma_{\tilde{h}}(t) = \left|\int_{t-T_s/2}^{t+T_s/2} \tilde{y}(t)s_{\tilde{h}}^{*}(t)\frac{\mathrm{d}\varphi_0(t)}{\mathrm{d}t}\mathrm{d}t\right|^2 \tag{11}$$

Rewriting the correlation functions, we obtain

$$\Gamma_{\tilde{h}}(t) = \left(\int_{t-T_s/2}^{t+T_s/2} R_{\tilde{h}}(t)\mathrm{d}t\right)^2 + \left(\int_{t-T_s/2}^{t+T_s/2} I_{\tilde{h}}(t)\mathrm{d}t\right)^2 \tag{12}$$

where

$$R_{\tilde{h}}(t) = \left\{\left[\cos\varphi(t)\cos\left(\tilde{h}\varphi_0(t)\right) + \sin\varphi(t)\sin\left(\tilde{h}\varphi_0(t)\right)\right]\frac{\mathrm{d}\varphi_0(t))}{\mathrm{d}t}\right\} \tag{13}$$

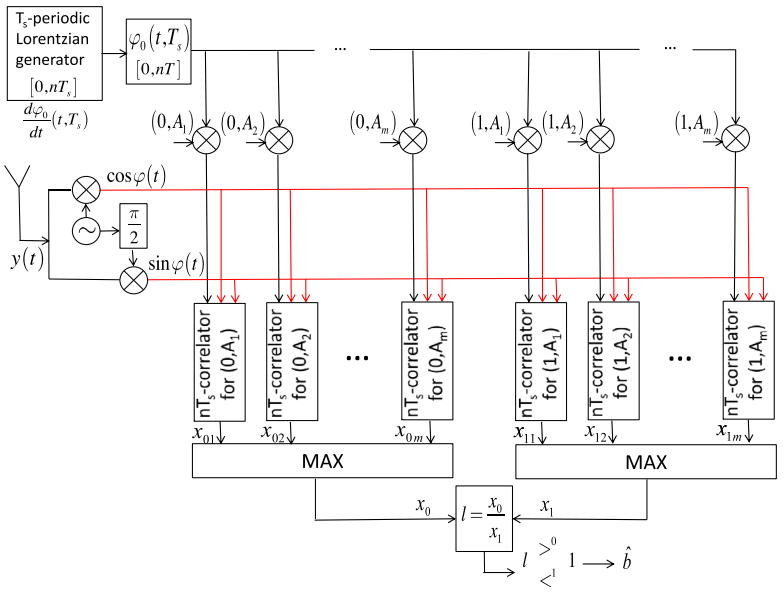

Fig. 4. Block diagram of the AMF-based detector.

and

$$I_{\tilde{h}}(t) = \left\{ \left[\sin\varphi(t) \cos\left(\tilde{h}\varphi_0(t)\right) - \cos\varphi(t) \sin\left(\tilde{h}\varphi_0(t)\right) \right] \frac{\mathrm{d}\varphi_0(t))}{\mathrm{d}t} \right\} \tag{14}$$

Finally, the correlation functions are then used in order to establish the likelihood ratio test

$$l = \frac{\Gamma_0}{\Gamma_h} \underset{<1}{\overset{>0}{}} 1 \tag{15}$$

4.3. Average matched-filter-based detector

Although its simplicity, the main drawback of MF-based detector is the inter-symbol interference (ISI), which is not taken into account. The AMF-based detector is then proposed to take advantage of the memory specific to CPM signals. The block diagram of the proposed AMF-based detector is shown in Fig. 4. The key idea consists in observing n symbols of an SSB–FSK waveform and producing a decision on one symbol. As the detector is coherent, the decision is made on the first symbol by observing the waveform during this symbol period and $n-1$ additional symbol periods.

The SSB–FSK modulated signal during the observation interval is denoted by $s(t, a_l, Ak)$, where A_k represents a particular symbol sequence, i.e. the $n-1$-tuple $a_2, a_3, ..., a_n$. The detection problem is then to observe $s(t, a_l, Ak)$ distorted by noise and produce a decision on a_1 (either 0 or 1).

Using the principles described in Sub-section 4.2 for symbol-by-symbol filtering and carrying out the integration over the nT_s observation intervals, the likelihood ratio becomes

$$l = \frac{\max\left\{ \left| \int_{-T_s/2}^{T_s/2} y(t) s^*(t, 0, A_1) \frac{\mathrm{d}\varphi_0(t)}{\mathrm{d}t} \mathrm{d}t \right|^2, ..., \left| \int_{-T_s/2}^{T_s/2} y(t) s^*(t, 0, A_m) \frac{\mathrm{d}\varphi_0(t)}{\mathrm{d}t} \mathrm{d}t \right|^2 \right\}}{\max\left\{ \left| \int_{-T_s/2}^{T_s/2} y(t) s^*(t, 1, A_1) \frac{\mathrm{d}\varphi_0(t)}{\mathrm{d}t} \mathrm{d}t \right|^2, ..., \left| \int_{-T_s/2}^{T_s/2} y(t) s^*(t, 1, A_m) \frac{\mathrm{d}\varphi_0(t)}{\mathrm{d}t} \mathrm{d}t \right|^2 \right\}} \tag{16}$$

In order to compute this likelihood ratio, the receiver correlates the received signal with each of the $m = 2^{n-1}$ possible transmitted signals followed by the symbol $a_k = 1$. A similar operation of correlation with the m possible transmitted signals followed by the symbol $a_k = 0$ is performed. Using the AMF-based detector improves the BER performance with a reasonable increase in complexity for reduced observation intervals.

5. Numerical results and comparisons

5.1. SSB Spectral property

In order to illustrate the single-sideband spectral property, we plot in Fig. 5 the power spectral density (PSD) of the SSB–FSK modulated signal averaged over 10 spectra corresponding to 10 streams of 2048 bits each. The analytical derivation

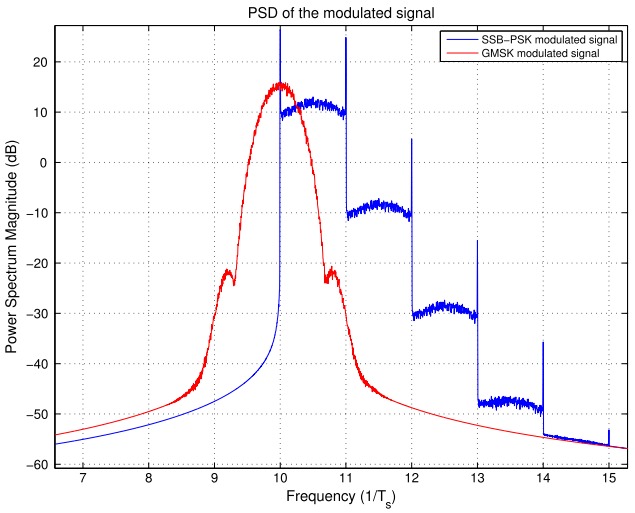

Fig. 5. Comparison of the power spectral densities: in blue for an SSB–FSK signal, in red for a GMSK signal, for the same carrier frequency $f_c = 10/T_s$.

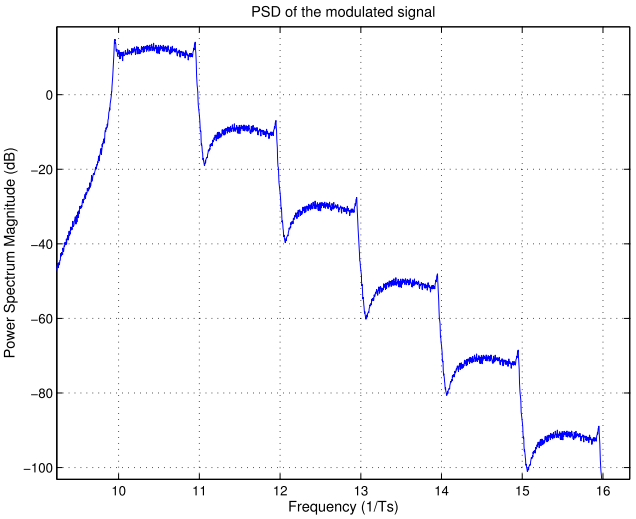

Fig. 6. Power spectral density of an SSB–FSK signal with 95% of the phase increment of a pure Lorentzian.

of this PSD has been detailed in [12]. For this illustration, non-truncated Lorentzian pulses of width $w = 0.37\,T_s$ are used, i.e. numerically, we choose a large enough L value to guarantee a phase increment equal to 2π (what corresponds to $\mu = 1$). The frequencies are in units of $1/T_s$. The carrier frequency is $f_c = 10/T_s$. In this example, we choose $h = 1$, a positive integer; as a result all the spectral components of the signal are located in the upper band with respect to f_c. For comparison, we also present the PSD of the GMSK modulated signal.

Comparing the PSDs of the SSB–FSK and the GMSK modulated signal, we can note that the PSD of the SSB–FSK is indeed unilateral and is no more symmetrical with respect to the carrier frequency f_c as for the GMSK case. Almost all of the power is concentrated in a $1/T_s$ frequency band and the power spectrum decreases steeply in steps of 20 dB, spaced by frequential periods of $1/T_s$. This exponential decrease is equal to $e^{-4\pi wf}$, which is equivalent to 1/100 in linear scale and to 20 dB in logarithmic scale for $w/T_s = 0.37$. This power exponential decay ($e^{-4\pi wf}$) of the SSB–FSK can be tuned by the Lorentzian width w. A trade-off on the value of w has to be found in order to balance, on one side, the ISI reduction by limiting w and to ensure, on the other side, a fast power decay outside the useful band by increasing w.

Furthermore, spikes at frequencies f_c, $f_c + 1/T_s$, $f_c + 2/T_s$, etc., are also present in the PSD illustration of the SSB–FSK. Their presence is an immediate consequence of the 2π phase increment, which is well known in conventional phase modulation techniques [13]. These spectral spikes can be removed by deviating a little from this critical value, at the cost of a reappearance of very low-amplitude components in the lower band. The PSD of the SSB–FSK with a phase increment equal to 95% of 2π is represented in Fig. 6. The configuration of the signals considered in Fig. 5 has been maintained for this illustration. The major difference is the clear reduction of the spectral spikes. However, its spectral occupation has slightly increased.

Table 1
Spectral occupation and correcting factor μ for different values of L.

SSB–FSK				
L	∞	12	4	2
μ	1	1.04	1.13	1.29
BW	1	1.08	1.26	1.53

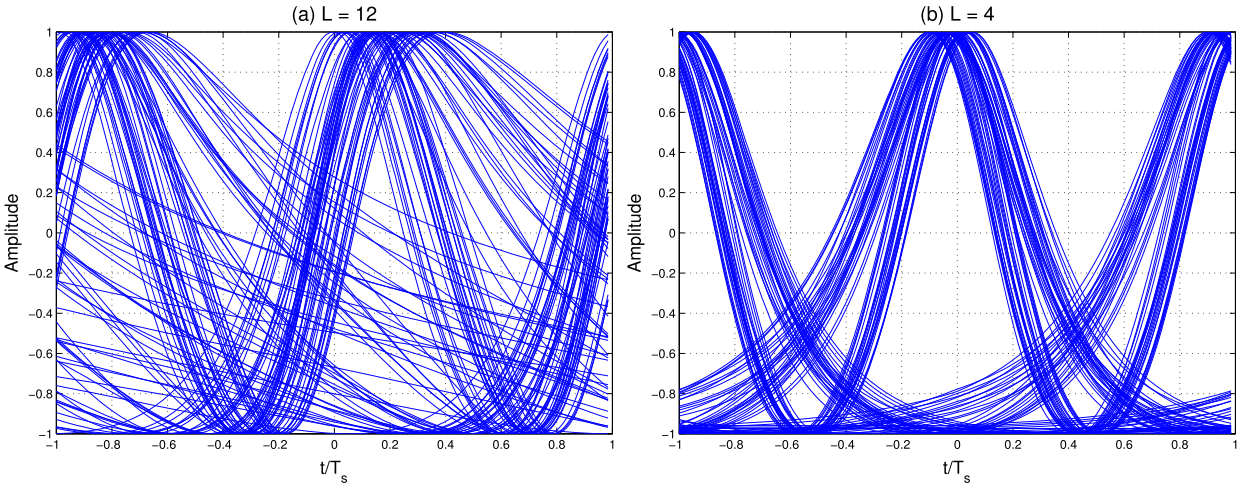

Fig. 7. Eye diagram of SSB–FSK modulated using Lorentzian pulses truncated to L symbol periods: (a) $L = 12$, (b) $L = 4$.

Table 1 provides the effect of the Lorentzian truncation on the PSD of the SSB–FSK modulated signal. In this table, we present the spectral occupation of the modulated signal for several values of $L = \infty, 12, 4, 2$.

This spectral occupation, denoted by BW, is expressed in terms of normalized frequency band $(1/T_s)$ occupied by 98% of the signal power transmitted for $w = 0.37T_s$. For comparison, we also give the spectral occupation of a GMSK signal. For instance, for $BT = 0.3$, $BW = 0.86$. We can clearly note through these results that, for non-truncated Lorentzian pulses, the spectral occupation of the SSB–FSK modulation remains close to those reached by the GMSK modulation. However, the more truncated the waveform is, the more spectral occupation increases.

5.2. Bit Error Rate performance

This sub-section investigates the performance of the SSB–FSK in terms of BER over an AWGN channel. As this particular performance metric is very sensitive to the ISI level, we first evaluate the impact of the Lorentzian pulse length on the ISI. To do so, we provide in Fig. 7 the eye diagram of the SSB–FSK signal for $L = 12$ and 4. We clearly observe much more interference between symbols for a truncation at $L = 12$ compared to $L = 4$. As a result, the demodulation of the signal passing through a noisy channel in the presence of the ISI level for $L = 12$ will be considerably less efficient compared to $L = 4$. From Table 1 and Fig. 7, a truncation of the Lorentzian at $L = 4$ periods seems to be a good compromise between the preservation of the spectral occupation (by conserving the SSB property) and the reduction of the ISI level.

In Fig. 8, we plot the BER curves of SSB–FSK modulation using MF-based detector for several Lorentzian pulse length values $L = 100, 4, 2$ as a function of E_b/N_0, the bit-energy-to-noise ratio. This quantifies the effect of truncation on the performance of the proposed demodulation scheme and thus its immunity against ISI. It is a non-surprising result that SSB–FSK modulation with the most severe truncation of the Lorentzian pulse is the most efficient, since it is subject to the lowest ISI level. A bound on the bit error probability is given in order to illustrate the potential of this new modulation. This performance bound is described using error events and minimum distance simulation [14,15]. In order to simulate the minimum distance relative to this modulation, we assume the following error event: we transmit the symbol sequence $\mathbf{a}_{Tx}$ and we receive the symbol sequence $\mathbf{a}_{Rx}$, defined both as

$$\begin{aligned} \mathbf{a}_{Tx} &= (\ldots, a_{e-1}, a_e, a_{e+1}) \\ \mathbf{a}_{Rx} &= (\ldots, a_{e-1}, \bar{a}_e, a_{e+1}) \end{aligned} \tag{17}$$

The phases of SSB–PSK modulated signals relative to both $\mathbf{a}_{Tx}$ and $\mathbf{a}_{Rx}$ information sequences diverge at position e and converge again due to the 2π phase increment. Consequently, the minimum Euclidean distance d_{min} is then relative to a

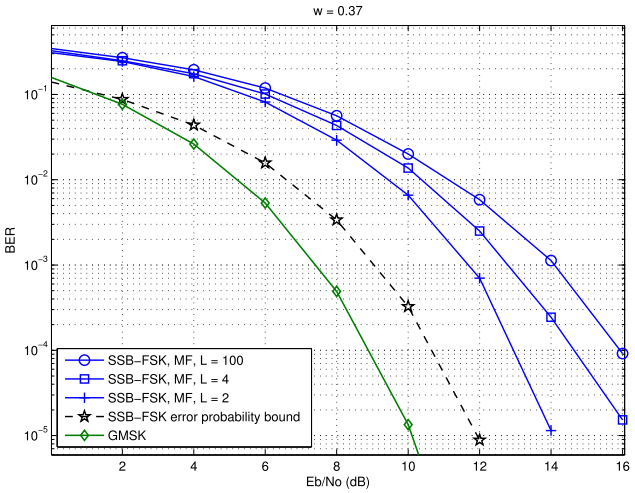

Fig. 8. BER performance of MF-based detector for several truncation scenarios $L = 100, 4, 2$.

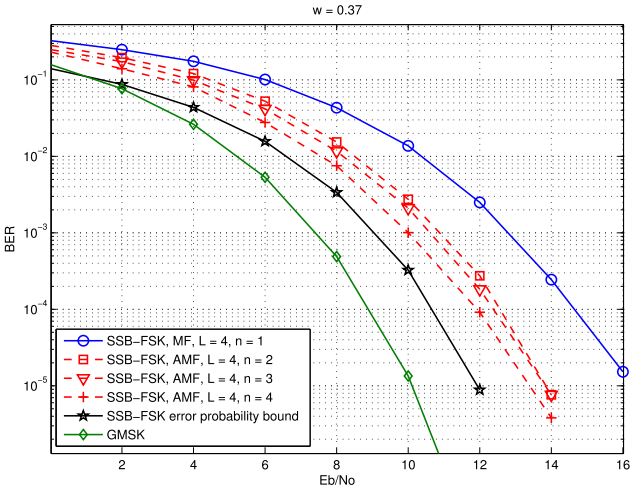

Fig. 9. BER performance of AMF-based detector for several observation interval values $n = 2, 3, 4$.

single-symbol error event. The probability of bit error is then bounded as

$$P_b \leq \frac{1}{2} Q\left(\sqrt{d_{\min}^2 \frac{E_b}{N_0}}\right) \tag{18}$$

where $Q(x) = \frac{1}{\sqrt{2\pi}} \int_x^\infty e^{-u^2/2}\, du$.

Furthermore, the BER curves of SSB–FSK modulation using an AMF-based detector for several observation interval values are given in Fig. 9 for $L = 4$ and are compared to the BER curve using an MF-based detector. For $n = 2$, a gain of almost 2 dB at BER $= 10^{-3}$ is offered with respect to the BER performance of the MF-based detector. Smaller gains are observed for larger values of n ($n = 3, 4$). The best performance of the AMF-based detector is given for $n = L$. However, even if the AMF-based detector is performing much better than the MF-based detector, this demodulation scheme is not the optimal one and it is still around 1 dB above the optimal performance.

Finally, even if SSB–FSK offers a lower BER performance compared to GMSK due to a higher amount of ISI caused by a significant overlap between Lorentzian pulses, the proposed waveform may be preferred in some specific transmission contexts. For instance, the total absence of lower sideband allows one to operate with a symbol rate $1/T_s$ much larger than the carrier frequency f_c, typically $4f_c$, without deterioration of the BER, as there is no interference with the mirror spectrum.

6. Conclusions

In this paper, we present a new single-sideband waveform. We explain the eve of this idea derived from quantum physics. Moreover, we compare its power spectral density with that obtained from a conventional continuous phase modulation (GMSK) widely used in transmission contexts that can be targeted by this new proposal. Being a partial response, like the GMSK, this waveform exhibits inter-symbol interference. A tradeoff between spectral occupation and demodulation efficiency in the presence of noise is then fixed. Two different demodulation schemes have been developed, and simulation results in terms of BER have been given in order to evaluate their potential. Since none of them achieves optimal performance, future work will focus on the Viterbi-based demodulation scheme using pulse amplitude modulation (PAM) decomposition. This is not straightforward since the proposed SSB–FSK scheme has an integer modulation index ensuring a 2π phase increment.

References

[1] R.V.L. Hartley, US patent 1666206.
[2] D.K. Weaver, A third method of generation and dectection of single-sideband signals, in: Proceeding of the IRE, 1956, pp. 1703–1705, https://doi.org/10.1007/978-1-4899-2031-7.
[3] J.B. Anderson, T. Aulin, C.E.W. Sundberg, Digital Phase Modulation, Plenum Press, New York, 1986.
[4] C.H. Kuo, K.M. Chugg, On the bandwidth efficiency of CPM signals, in: Proc. IEEE Military COmm. Conf. (MILCOM), 2004, pp. 218–224.
[5] R.P.G. McNeil, M. Kataoka, C.J.B. Ford, C.H.W. Barnes, D. Anderson, G.A.C. Jones, I. Farrer, D.A. Ritchie, On-demand single-electron transfer between distant quantum dots, Nature 477 (2011) 43–442, https://doi.org/10.1038/477414a.
[6] G. Fève, A. Mahé, J.M. Berroir, T. Kontos, B. Plaçais, D.C. Glattli, A. Cavanna, B. Etienne, Y. Jin, An on-demand coherent single-electron source, Science 316 (2007) 1169–1172, https://doi.org/10.1126/science.1141243.
[7] N. Ubbelohde, F. Hohls, V. Kashcheyevs, T. Wagner, L. Fricke, B. Kastner, K. Pierz, H.W. Schumacher, R.J. Haug, Partitioning of on-demand electron pairs, Nat. Nanotechnol. 10 (2015) 46–49, https://doi.org/10.1038/nnano.2014.275.
[8] J. Dubois, T. Jullien, F. Portier, P. Roche, A. Cavanna, Y. Jin, W. Wegscheider, P. Roulleau, D.C. Glattli, Minimal-excitation states for electron quantum optics using levitons, Nature 502 (2013) 659–663, https://doi.org/10.1038/nature12713.
[9] T. Jullien, P. Roulleau, B. Roche, A. Cavanna, Y. Jin, D. Glattli, Quantum tomography of an electron, Nature 514 (2014) 603–607, https://doi.org/10.1038/nature13821.
[10] L.S. Levitov, H. Lee, G. Lesovik, Electron counting statistics and coherent states of electric current, J. Math. Phys. 37 (1996) 4845, https://doi.org/10.1063/1.531672.
[11] D.C. Glattli, P. Roulleau, patent wo2016124841 a1.
[12] H. Farès, D.C. Glattli, Y. Louet, J. Palicot, P. Roulleau, C. Moy, Power spectrum density of single side band CPM using lorenztian frequency pulses, IEEE Wirel. Commun. Lett. 6 (6) (Dec. 2017) 786–789, https://doi.org/10.1109/LWC.2017.2742505.
[13] H.E. Rowe, V.K. Prabhu, Power spectrum of a digital frequency-modulation signal, Bell Syst. Tech. J. 54 (1975) 1095–1125, https://doi.org/10.1002/j.1538-7305.1975.tb02884.x.
[14] E. Perrins, M. Rice, Reduced-complexity approach to iterative detection of coded SOQPSK, IEEE Trans. Commun. 55 (2007) 13541362, https://doi.org/10.1109/TCOMM.2007.900614.
[15] H. Farès, D.C. Glattli, Y. Louet, C. Moy, J. Palicot, P. Roulleau, New binary single side band CPM, in: Proc. IEEE International Conference on Telecommunications, ICT, 2017.